


## Carbon vacancy-related centers in 3C-silicon carbide: Negative- $U$ properties and structural transformation

H. J. von Bardeleben

*Sorbonne Université, Institut des Nanosciences de Paris, UMR 7588 au CNRS 4, place Jussieu, 75005 Paris, France*

E. Rauls

*University of Stavanger, Institutt for Matematikk og fysikk, Kristine Bonnevisvei 22, 4036 Stavanger, Norway*

U. Gerstmann 

*Department Physik, Universität Paderborn, Warburger Straße 100, 33098 Paderborn, Germany*



(Received 31 January 2020; revised manuscript received 10 April 2020; accepted 20 April 2020; published 11 May 2020)

Combining electron paramagnetic resonance (EPR) spectroscopy and first-principles density functional theory calculations we have identified the carbon monovacancy center and a second carbon vacancy-related defect, the carbon vacancy–carbon antisite defect in 3C-SiC. In close analogy to the vacancy in silicon, the carbon vacancy in 3C-SiC with its four potentially equivalent silicon dangling bonds shows a strong Jahn-Teller effect, confirming previously predicted negative- $U$  properties. High-temperature annealing (above 700 °C) of electron or proton irradiated samples anneals out the primary silicon monovacancies and generates a new defect, which we assign to the carbon vacancy–carbon antisite complex. As predicted by theory, this defect is the result of a structural instability of the silicon vacancy in the positive charge state, which transforms at high temperatures according to  $V_{\text{Si}}\text{C}_4 \rightarrow V_{\text{C}}\text{C}_{\text{Si}}\text{C}_3$ . Both defects are deep donors and thus not suitable for achieving semi-insulating properties.

DOI: [10.1103/PhysRevB.101.184108](https://doi.org/10.1103/PhysRevB.101.184108)

### I. INTRODUCTION

Among the intrinsic defects in silicon carbide, vacancies and interstitials are the most-simple conceptual ones and are also the building blocks of more complex defects such as divacancies or vacancy-donor associates. Their study is of fundamental and technological interest as they modify the electrical and optical properties. In the hexagonal polytypes 4H and 6H both silicon and carbon vacancy-related defects have been investigated in much detail, both experimentally ([1–8]; for a recent review, see Ref. [9]) and by theory [10–16]. This is not the case of the cubic polytype 3C-SiC, where the carbon monovacancy, for example, has escaped any detection. We focus in this study on the investigation of carbon vacancy-related defects introduced by particle irradiation.

Even though the observation of a paramagnetic defect (T5) attributed to the carbon monovacancy in 3C-SiC has been reported many years ago by Itoh *et al.* [1], this assignment has been shown to be erroneous. The first assignment had been made in the absence of any modeling. In 2002, Petrenko *et al.* [4] showed, based on the analysis of the experimental hyperfine interactions, that the T5 center is actually the positively charged carbon-split interstitial (C-C)<sub>C</sub>, which is the stable configuration of the carbon interstitials in all SiC polytypes. Since then, i.e., for nearly two decades, no new experimental observation concerning the carbon monovacancy in 3C-SiC has been reported. In other words, a clear experimental fingerprint of the isolated carbon vacancy in 3C-SiC was still

missing. Theory has predicted the carbon monovacancy to have multiple stable charge states ranging from 1– to 1+ in all three polytypes [10–15]. Both the 1– and 1+ charge states are paramagnetic with spin  $S = 1/2$  ground states and should thus be observable by electron paramagnetic resonance spectroscopy (EPR); in the neutral charge state both  $S = 0$  and spin  $S = 1$  ground states had been predicted. Here we report the observation and identification of this defect in the 1+ charge state.

In the second part of this work we have investigated a second carbon vacancy-related defect in 3C-SiC. It is produced by the structural transformation of the silicon monovacancy defect at high temperature: by a nearest-neighbor hop of a carbon atom near a silicon vacancy a carbon vacancy–carbon antisite complex is formed. This instability had been previously predicted in 3C-SiC by theory but not evidenced by experiments.

An additional motivation for this work is the recent interest in the application of intrinsic defects in SiC in quantum technology as qubits [17–24] and nanoscale sensors for temperature and magnetic fields [25,26]. In 3C-SiC the divacancy and the nitrogen-vacancy (NV) center [22,23] have been particularly studied; very recently the carbon vacancy–carbon antisite defect in 3C-SiC has also been suggested to be a promising single-photon source [26], but this assignment had still to be confirmed.

In this work we have applied particle irradiation for the controlled formation of the carbon and silicon vacancy-related

intrinsic defects and investigated by combined EPR spectroscopy and *ab initio* calculations their microscopic and electronic structure.

## II. EXPERIMENTAL DETAILS

In this study we used commercially purchased (Hoya Corp., Japan) 250- $\mu\text{m}$ -thick (100)-oriented nitrogen-doped *n*-type 3C-SiC samples as starting material. The carrier concentration is in the  $2 \times 10^{17}\text{cm}^{-3}$  range. The samples were cut to typical dimensions of  $4 \times 5\text{mm}^2$ . They were irradiated at room temperature either with high-energy electrons (0.3...2 MeV) or protons (2 MeV) to fluencies up to  $10^{18}\text{cm}^{-2}$ . The samples were kept at room temperature and their defect properties were found to be stable over months. Some of the samples were annealed at high temperature (700°C–900°C) to investigate the thermal stability of the defects. In particular, we wanted to study the predicted instability of the silicon monovacancy in the 700°C temperature range. Therefore some samples were furnace annealed between 700°C and 900°C in an inert atmosphere. The EPR measurements were performed with a commercial BrukerX-band (9 GHz) spectrometer in the temperature range between 4 and 300 K. The spectra were recorded in a standard way with 100 kHz field modulation and lock-in detection. The spectra were measured either under thermal equilibrium conditions or under *in situ* photoexcitation. For the photoexcitation we disposed of different diode lasers in the 650–980 nm range with maximum 100 mW output. The angular variations of the EPR spectra were simulated with the program “Visual EPR” from Grachev [27].

## III. COMPUTATIONAL DETAILS

The calculations of the spin Hamiltonian parameters for reasonable carbon vacancy-related defects were performed within density functional theory (DFT). The defect structures were modeled with 512-atom 3C-SiC supercells using the QUANTUM ESPRESSO software [28,29]. The hyperfine (hf) coupling constants as well as the elements of the electronic *g* tensors were calculated with the GIPAW module of QUANTUM ESPRESSO [28] using a shifted  $3 \times 3 \times 3k$ -point sampling. We have used the Perdew-Burke-Ernzerhof (PBE) functional [30] for both geometry optimization and EPR parameter calculation along with norm-conserving pseudopotentials and a plane-wave (PW) basis set with kinetic-energy cutoff of 90 Ry. For the calculation of charge transition levels, however, we use the concept of the Slater-Janak transition state [31,32] together with the PBE + *U* approach, whereby a *U* value of 4.7 eV was applied onto the carbon *2p* electrons, in order to adjust the fundamental gap to the experimental value of 2.39 eV. In GaN, the same approach was shown to provide charge transition levels in very good agreement with those predicted by a hybrid functional [33]. For small 64-atom supercells we evaluated this method for the present 3C-SiC case against fully relaxed Heyd-Scuseria-Ernzerhof calculations [34] and obtain within 5% the same (i.e., slightly smaller) charge transition levels and excitation energies. For the large 512-atom supercell, the PBE + *U* approach allows a structurally fully relaxed self-consistent field treatment, where

such an application of hybrid functionals is still prohibitively expensive.

## IV. RESULTS AND DISCUSSION

Before irradiation the samples display only the EPR spectrum of the neutral nitrogen donor [35]. After irradiation we observe two previously identified defects: (i) the negatively charged silicon vacancy  $V_{\text{Si}}^-$ , a high-symmetry, high-spin  $S = 3/2$  center with vanishing magnetic anisotropy ( $D = 0$ ) [1] and (ii) the positively charged carbon dumbbell  $(\text{C-C})_{\text{C}}^+$  [4], a spin  $S = 1/2$  defect. As both spectra have been reported before, they will no longer be discussed here.

Under photoexcitation at low temperature we observe in addition a new spin  $S = 1/2$  center, which is the object of this study. It is characterized by an unusual tetragonal point symmetry  $D_{2d}$ . We assign this center as shown in the following to the carbon monovacancy in the 1+ charge state ( $V_{\text{C}}^+$ ). When the irradiated samples were annealed at high temperature (700°C–900°C), the silicon monovacancy  $V_{\text{Si}}^-$  and the carbon dumbbells (split interstitials) were no longer observed. Instead an additional new spin  $S = 1/2$  center was generated, which we attribute to the positively charged carbon vacancy–carbon antisite complex.

### A. Carbon monovacancy

In Fig. 1(a), we show a typical EPR spectrum of an irradiated, nonannealed sample before and under photoexcitation at  $T = 4$  K. Before photoexcitation we observe the nitrogen shallow donor spectrum with spin  $S = 1/2$ , which displays a triplet structure due to the hf interaction with  $^{14}\text{N}$  nucleus [35]. Under photoexcitation a new irradiation-induced EPR spectrum is superimposed. It is characterized by a much smaller linewidth of  $\Delta B_{pp} = 200$  mG. For the orientation of the magnetic field parallel to the [001] axis, this spectrum is composed of two lines with an intensity ratio 1:2 and *g* values of  $g_1 = 2.0026$  and  $g_2 = 2.0064$ , respectively. For an arbitrary orientation of the magnetic field in the (110) plane the spectrum is composed of two lines. In Fig. 1(b) we show the experimental results of the angular variation of the resonance fields for a rotation of the magnetic field in the (110) plane. This angular variation of the EPR spectrum demonstrates an unusual tetragonal point symmetry  $D_{2d}$  which can be fitted with the spin-Hamiltonian parameters  $S = 1/2$  and an axial *g* tensor with principal values  $g_{\parallel 100} = 2.0064$  and  $g_{\perp 100} = 2.0024$  (Fig. 1).

The small linewidth allows us to resolve also hyperfine interactions, a key parameter for establishing a microscopic model. We observe both central (chf) hyperfine and superhyperfine (shf) lines, the intensities of which are characteristic for the interaction of the electron spin with 4 Si atoms and 12 C atoms, respectively [cf. Fig. 1(c)]. This intensity distribution is characteristic for a carbon site defect, which has 4 Si nearest neighbors and 12 C next-nearest neighbors. The strongest chf interaction is with the nearest Si neighbors. The chf interaction could be resolved for  $B \parallel [001]$  and  $B \parallel [111]$  (Table I). For  $B \parallel [001]$  the experimental value is  $42 \times 10^{-4}\text{cm}^{-1}$ . The shf parameter is nearly isotropic and has a value of about 3.5 G (for further details, see Table I).

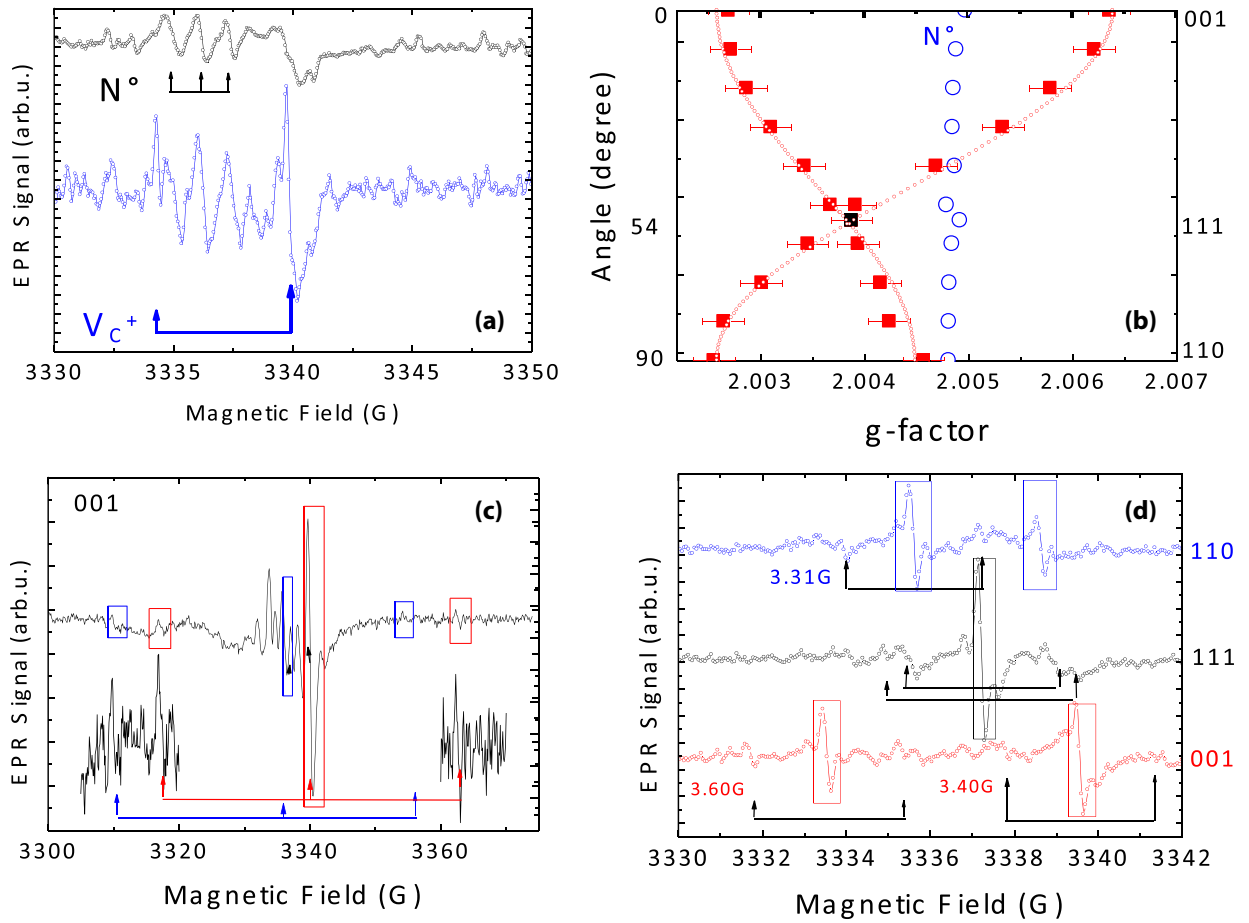


FIG. 1. (a) EPR spectrum of the  $V_C^+$  center in electron-irradiated 3C-SiC: (top) before excitation only the neutral  $N^\circ$  spectrum is observed; (bottom) photoexcitation generates the  $V_C^+$  spectrum and increases the intensity of  $N^\circ$ ;  $T = 4$  K and  $B \parallel [001]$  (b) Experimental (red squares) and simulated (red circles) angular variation of the  $V_C^+$  EPR spectrum and the isotropic spectrum of  $N^\circ$  (blue circles). (c) EPR spectrum for  $B \parallel [001]$  showing the central hyperfine interaction with  $^{29}\text{Si}$ . (d) EPR spectra of the  $V_C^+$  center for three orientations of the magnetic field showing the resolved superhyperfine (shf) interaction (in G) with  $^{29}\text{Si}$ ;  $T = 4$  K.

TABLE I. Spin-Hamiltonian (EPR) parameters (experimental and calculated) of the positively charged carbon vacancy  $V_C^+$  in 3C-SiC and, for comparison, those of the positively charged silicon vacancy  $V_{\text{Si}}^+$  in Si (G1 center).

Material	$V_{\text{Si}}^+$ (G1) Silicon	$V_C^+$ 3C-SiC
Spin	1/2	1/2
Symmetry	$D_{2d}$	$D_{2d}$
$g$ tensor,	$g_{\parallel 100} = 2.0087$	$g_{\parallel 100} = 2.0064$
Expt.	$g_{\perp 100} = 1.9989$	$g_{\perp 100} = 2.0026$
Theory (this work)	$g_{\parallel 100} = 2.0076$	$g_{\parallel 100} = 2.0067$
	$g_{\perp 100} = 1.9982$	$g_{\perp 100} = 2.0023$
$^{29}\text{Si}$ chf,	$ A_{\parallel}  = 43.9 \times 10^{-4} \text{ cm}^{-1}$	$ A_{\parallel 001}  = 42 \times 10^{-4} \text{ cm}^{-1}$
Expt. ( $10^{-4} \text{ cm}^{-1}$ )	$ A_{\perp}  = 29.8 \times 10^{-4} \text{ cm}^{-1}$	$ A_{\parallel 111}  : 51 \times 10^{-4} \text{ cm}^{-1} / 40 \times 10^{-4} \text{ cm}^{-1} / 37 \times 10^{-4} \text{ cm}^{-1}$
Theory ( $10^{-4} \text{ cm}^{-1}$ )	$A_{33} = -43.7 \times 10^{-4} \text{ cm}^{-1}$	$A_{33} = -54.7 \times 10^{-4} \text{ cm}^{-1}$
(this work)	$A_{22} = -31.4 \times 10^{-4} \text{ cm}^{-1}$	$A_{22} = -38.8 \times 10^{-4} \text{ cm}^{-1}$
	$A_{11} = -30.8 \times 10^{-4} \text{ cm}^{-1}$	$A_{11} = -38.1 \times 10^{-4} \text{ cm}^{-1}$
		$ A_{\parallel 001}  = 41.8 \times 10^{-4} \text{ cm}^{-1}$
		$ A_{\parallel 111}  : 54 \times 10^{-4} \text{ cm}^{-1} / 42 \times 10^{-4} \text{ cm}^{-1} / 39 \times 10^{-4} \text{ cm}^{-1}$
$^{29}\text{Si}$ shf, expt.		$A_{\text{SHF, expt.}} = 3.3 \dots 4.5 \text{ G}$
theory (this work)		$A_{\text{SHF, DFT}} = 3.3 \dots 4.9 \text{ G}$

TABLE II. Predicted carbon monovacancy ground-state properties in 3C-SiC: Besides total spin  $S$ , symmetry, and related Jahn-Teller energies (up to 0.5 eV), the charge transition levels are given, with  $(+/0) < (2+/+)$ , i.e., a strong negative- $U$  effect and direct  $(2+/0)$  recharging at  $E_{VB} + 1.61$ . We note that in silicon (this work) and 4H-SiC [10] much smaller Jahn-Teller energies (below 0.2 eV) are calculated.

Charge state	2+	+	0
Total spin $S$	0	1/2	0
(Point group) symmetry	$T_d$	$D_{2d}(C_{3v} - 0.042 \text{ eV})$ $(T_d - 0.203 \text{ eV})$	$D_{2d}(C_{3v} - 0.321 \text{ eV})$ $(T_d - 0.503 \text{ eV})$
Charge transition levels		$(2+/+) = E_{VB} + 1.73 \text{ eV}$	$(+/0) = E_{VB} + 1.52 \text{ eV}$

An obvious candidate for this center is the carbon monovacancy in the 1+ charge state (Table II). Indeed, the carbon vacancy is an expected primary irradiation-induced defect and its presence is indirectly indicated by the observation of carbon dumbbell centers. Early cluster calculations by Petrenko *et al.* [11] of the  $V_C^+$  center in 3C-SiC had already predicted a  $D_{2d}$  symmetry and a central hf interaction ( $^{29}\text{Si}$ ) with hf parameters  $a_{\text{iso}} = -40 \times 10^{-4} \text{ cm}^{-1}$  and anisotropy parameter  $b$  of  $-8 \times 10^{-4} \text{ cm}^{-1}$ . Bockstedte *et al.* [13] refined these calculations with more reliable supercell data; they obtained a larger isotropic hf contribution ( $a_{\text{iso}} = -47 \times 10^{-4} \text{ cm}^{-1}$ ) and a slightly smaller anisotropy parameter  $-7 \times 10^{-4} \text{ cm}^{-1}$ . Our present *ab initio* supercell calculations (in 512-atom supercells) provide a complete set of EPR parameters, i.e., the hf interaction parameters as well as the principal values of the electronic  $g$  tensors. As shown in Table I, both the principal values of the  $g$  tensor as well as the hyperfine interaction parameters are in good agreement with the experimental values. We thus attribute this defect to  $V_C^+$ .

We have further studied the spectral dependence of the photoexcitation required to generate the  $V_C^+$  state at some selected wavelengths. Photoexcitation at 650, 808, and 980 nm generate the  $V_C^+$  center in a similar way. The photoinduced generation of the  $V_C^+$  center is accompanied by an increase in the neutral donor concentration which indicates a photoionization  $V_C^0 \rightarrow V_C^+ + e_{cb}$  to the conduction band and subsequent capture by ionized shallow donors. Our calculations show an ionization threshold of 0.8 eV, which is coherent with the observation that excitation at wavelengths between 650 and 980 nm are efficient (Table II). After photoexcitation at  $T = 4 \text{ K}$ , the center is metastable up to  $T = 50 \text{ K}$ .

A tetragonal point symmetry is unusual for intrinsic defects in 3C-SiC. Our calculations show that it is due to a strong Jahn-Teller effect (Table II). A similar effect has also been reported for the silicon monovacancy in silicon, the isostructural variant of the  $V_C$  center in 3C-SiC [36–39]. This defect has basically the same microscopic and electronic structure (Fig. 2). We have thus compared the EPR parameters and magnetization density of the two defects in Table I and Fig. 2, respectively; the parameters for the  $V_{\text{Si}}$  in silicon have also been recalculated in this work.

The stable configurations of  $V_C$  in the three different charge states  $(-/0/+)$  are shown in Table II and Fig. 3(d). As in the case of  $V_{\text{Si}}$  in Si, the carbon vacancy is surrounded by four nearest Si neighbors, whose hybridized dangling bond states form the electronic ground state. Already in silicon, the interaction between the Si dangling bonds gives rise to strongly charge-state depending Jahn-Teller distortions [36].

For  $V_C$  in 3C-SiC this effect is even stronger due to the smaller lattice constants; relative to undistorted  $T_d$  symmetry energies of 0.2 eV for the positive, and even 0.5 eV for the neutral charge state are gained by a pairwise coupling of the Si dangling bonds (see Fig. 2, middle), resulting in the  $D_{2d}$  symmetry. This exceptionally strong Jahn-Teller distortion for the neutral charge state makes its diamagnetic configuration 0.3 eV more stable than any paramagnetic variant. It leads to a direct recharging from the 2+ to the neutral charge state [see also Table II and Fig. 3(d)], making the 2+ and 0 diamagnetic charge states the only stable ones. In contrast to the case of  $V_C$  in the hexagonal SiC polytypes, the negative charge state is found in 3C-SiC already deep in the conduction band.

### B. Carbon vacancy–carbon antisite pair $V_C C_{\text{Si}}$

To investigate the predicted instability of the  $V_{\text{Si}}$  defect and its transformation into the  $V_C C_{\text{Si}}$  centers [40–47] as well as the stability of the  $V_C$  center, we have studied the effect of high-temperature annealing on the irradiated samples, which contain  $V_{\text{Si}}$  and  $V_C$  as irradiation-induced primary defects. The samples were furnace annealed at  $T \geq 700^\circ$ , the temperature range for which annealing of the  $V_{\text{Si}}$  have been reported.

After annealing, the EPR spectrum of the  $V_C^+$  center is still observed after photoexcitation at  $T = 4 \text{ K}$ . The  $V_C$  defect is stable at annealing at  $T = 700^\circ \text{C}$ . In addition, we observe a new spin  $S = 1/2$  center [see Fig. 3(a)]. Its EPR spectrum is observable without photoexcitation and can be observed in the whole investigated temperature range from  $T = 4 \text{ K}$  to room temperature. The angular variation of the EPR spectra for a rotation of the magnetic field in the (110) plane reveals a trigonal  $C_{3v}$  symmetry, a  $g$  tensor with principal values of  $g_{\parallel 111} = 2.0023$  and  $g_{\perp 111} = 2.0037$ , and a nearly isotropic hyperfine interaction of about 20 G with three Si neighbors (see Table IV and Fig. 3).

To verify the model of a  $V_C C_{\text{Si}}$  center, we have calculated the spin states and EPR parameter for this defect in its different charge states. In Table III we show the calculated charge transition levels of this defect in 3C-SiC: we obtain three transitions  $(2+/+)$ ,  $(+/0)$ , and  $(0/-)$  at energies of  $E_V + 1.57$ ,  $E_V + 2.24$ , and  $E_V + 2.39 \text{ eV}$ . The  $V_C C_{\text{Si}}$  center is paramagnetic in the three charge states  $+/0/-$ , with the neutral charge state providing a ( $S = 1$ ) spin triplet and the + and – charge states being characterized by spin  $S = 1/2$  ground states. As the  $(0/-)$  charge transition level is degenerate with the conduction band, the negative charge state is probably unstable. The stable charge states are then  $2+/+/0$  and their occupation will depend on the Fermi level position. In



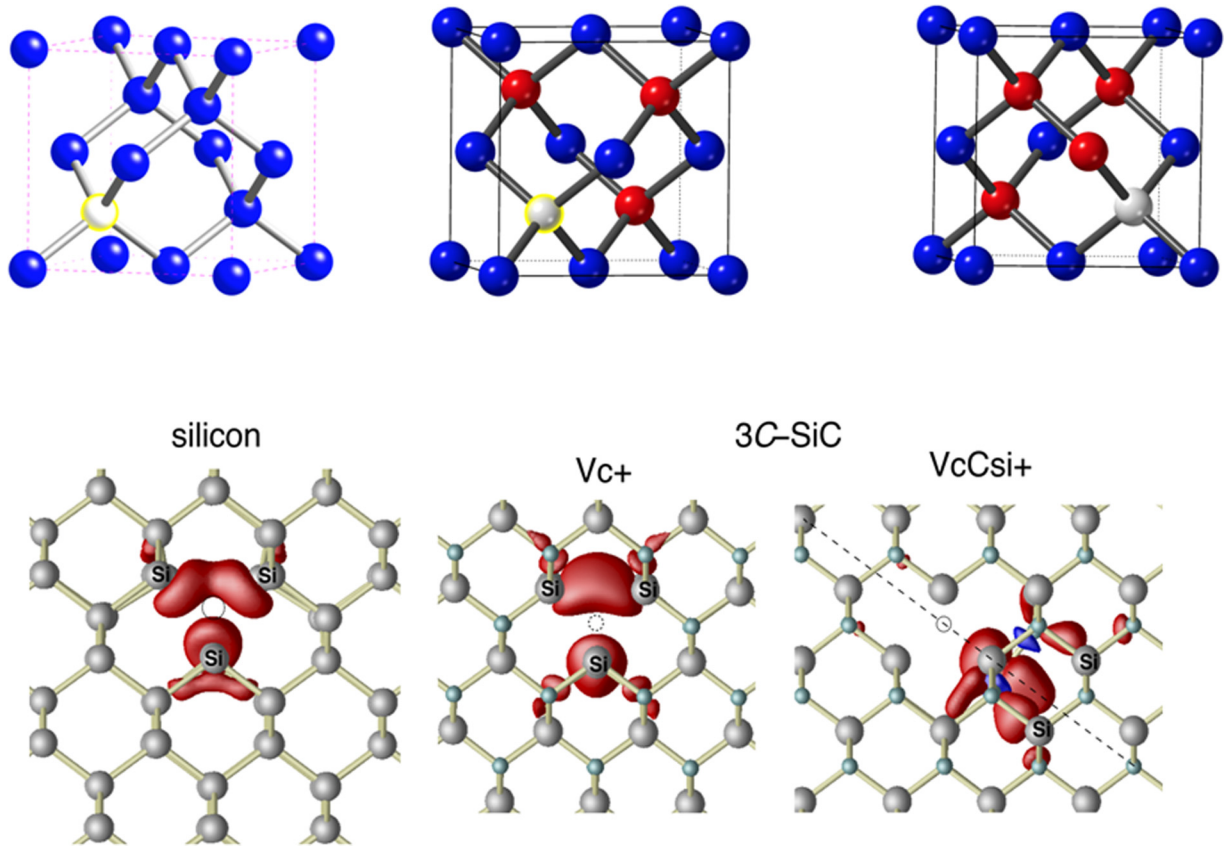


FIG. 2. Top: Crystal structure of the  $V_{\text{Si}}$  in Si,  $V_{\text{C}}$  in 3C-SiC, and  $V_{\text{C}}C_{\text{Si}}$  in 3C-SiC; vacancies, light gray; Si atoms, blue; carbon atoms, red. Bottom: Atomic structure and calculated magnetization density for the  $V_{\text{C}}^{+}$  (middle) and  $V_{\text{C}}C_{\text{Si}}^{+}$  (right)  $S = 1/2$  centers (“missing” atoms indicated by circles). For comparison, the isostructural monovacancy  $V_{\text{Si}}^{+}$  in silicon (24% larger lattice constant) is also shown (left). The Si nuclei giving rise to the experimentally resolved  $^{29}\text{Si}$  hyperfine (hf) splittings (cf. Tables I and IV) are indicated.

semi-insulating samples the  $V_{\text{C}}C_{\text{Si}}$  center should be observable in the 0 or 1+ charge state under thermal equilibrium conditions. Only the 1+ charge state is compatible with the observed spin  $S = 1/2$  center. In Table IV we compare the calculated spin Hamiltonian parameters of the  $V_{\text{C}}C_{\text{Si}}^{+}$  center and those of the annealing-induced new spin  $S = 1/2$  center. Clearly its point symmetry,  $g$  tensor, and the  $^{29}\text{Si}$ -related hf splittings are all in excellent agreement, which allows us to assign this defect to  $V_{\text{C}}C_{\text{Si}}$  in the 1+ charge state. The potentially *metastable* (see Table III) negative charge state is characterized by a different  $g$  tensor and a qualitatively different hf signature (see Table IV). In contrast to the case of the isolated  $V_{\text{C}}$ , our calculations for  $V_{\text{C}}C_{\text{Si}}$  show no significant negative- $U$  effect: with values around 90 meV (with respect to the “native”  $C_{3v}$  symmetry) the Jahn-Teller energies are much smaller.

### C. Defect interactions

The structural instability of the silicon monovacancy in  $p$ -type SiC and its transformation into the carbon antisite-carbon vacancy complex has been predicted in numerous theoretical studies, first for the hexagonal  $4H$  and  $6H$  polytypes [40,41], and later also for the cubic  $3C$  polytype [42–46]. This transformation operates easiest in  $p$ -type material, i.e., for the positive charge states, but depending on Si-/C-rich growth conditions and the polytype it remains possible for Fermi

levels up to 2 eV [48], i.e., for the 2+ to  $-$  charge states of  $V_{\text{Si}}$  [see also Fig. 3(d)]. In any case it requires high temperatures to overcome an energy barrier [40,46]. Thus, the initial  $n$ -type doping level and the irradiation-induced electrical compensations are two parameters, which will govern the instability or stability of the  $V_{\text{Si}}$  center under the annealing conditions. Our observation conclusively confirms the theoretically predicted structural instability of the silicon vacancy in cubic 3C-SiC.

Previously it has been shown that the annealing of irradiated  $n$ -type 3C-SiC in the same temperature range leads also to the formation of two spin  $S = 1$  centers, the neutral divacancy  $V_{\text{Si}}V_{\text{C}}^0$  [16] and the negatively charged NV center ( $V_{\text{Si}}N_{\text{C}}^{-}$ ) [22,23]. Their formation has been attributed to the mobility of the  $V_{\text{Si}}$ , which diffuses and interacts with stable  $V_{\text{C}}$  and  $N_{\text{C}}$  centers. Combining these results with our findings, the following scenario can be retained: parallel to the structural transformation of the  $V_{\text{Si}}$  center, it becomes mobile and forms complexes with carbon vacancies and nitrogen donors. Both processes are apparently operative at 700 °C annealing, and the resulting fractions will depend on the doping level and the electrical compensation of the samples.

Finally, we comment on the recent proposition that the  $V_{\text{C}}C_{\text{Si}}$  center in 3C-SiC might be a potentially interesting single-photon emitter with promising properties suitable for quantum technology applications [26]. These authors studied the room temperature photoluminescence of

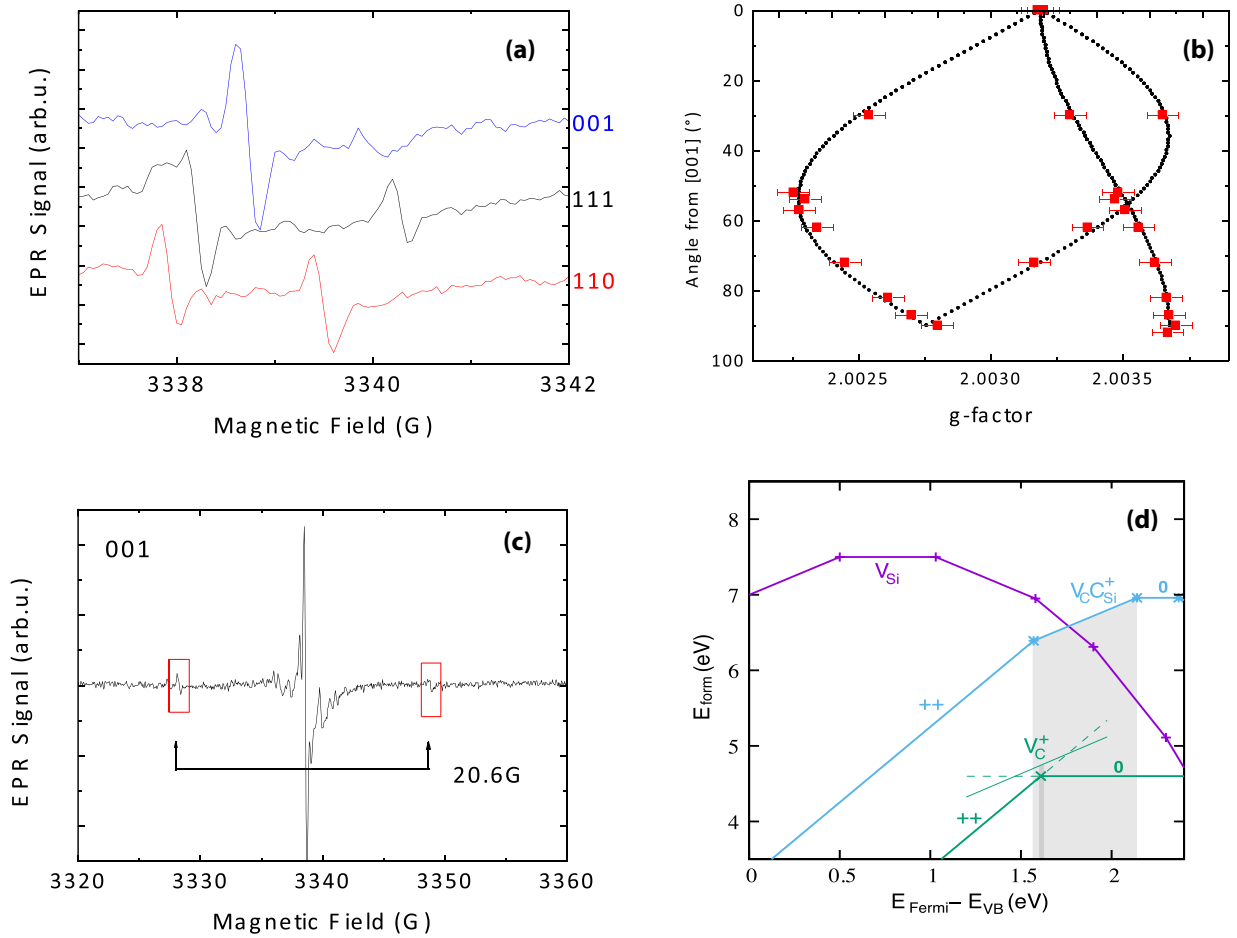


FIG. 3. (a) EPR spectra of the  $V_C C_{Si}^+$  center taken for three orientations of the magnetic field. (b) Angular variation of the  $V_C C_{Si}^+$  EPR spectra (red squares) in the [110] plane and its simulation (black circles) with the parameters: point symmetry  $C_{3v}$ ;  $g_{\parallel[111]} = 2.0023$ ,  $g_{\perp[111]} = 2.0037$ . (c)  $^{29}\text{Si}$  central hf interaction of the  $V_C C_{Si}^+$  center; resolved for  $B \parallel [001]$  at  $T = 80$  K. (d) Formation energies (eV) for the  $V_C$ -related defects in 3C-SiC ( $V_C$  and  $V_C C_{Si}$ ) in their possible charge states (given by the slope of the curves); EPR active  $S = 1/2$  centers identified in this work are indicated by areas shaded gray. The negative- $U$  effect for the metastable  $V_C^+$  is clearly visible (for details, see text and Table II). For comparison, the data for the isolated silicon vacancy  $V_{Si}$  is also given, showing the bistable, strongly Fermi-level-dependent nature of the ( $V_C C_{Si} \rightleftharpoons V_{Si}$ ) center.

cubic 3C-SiC nanoparticles and observed a broad Gaussian photoluminescence band centered at 650 nm, which they attributed tentatively to the  $V_C C_{Si}$  defect. It is characterized by an exceptionally strong single-photon emission with a record saturation count of  $7 \times 10^6$  counts/s, which makes this center an exceptional single-photon emitter. These authors relate this emission to the “ $E$ ” center zero-phonon line (ZPL) observable at low temperature. This model contradicts previous conclusions that the  $E$  line ZPL, which has been studied in quite some detail in irradiated bulk 3C-SiC, is associated with the

silicon monovacancy [48]. We have therefore also calculated the optical transitions of the  $V_C C_{Si}$  center in its various charge states. In light of our theoretical results the assignment of a ZPL at 1.95 eV ( $E$  line) in 3C-SiC nanoparticles to  $V_C C_{Si}$  centers seems highly improbable: our total energy calculations and subsequent analysis of the Slater-Janak transition states, situates the  $(2+/+)$  and  $(+/0)$  charge transition levels of the  $V_C C_{Si}$  center at  $E_v + 1.57$  eV and  $E_v + 2.24$  eV, placing any intracenter transitions with energies of 1.95 eV highly resonant with the conduction band. This makes an efficient

TABLE III. DFT-predicted properties of the carbon vacancy–carbon antisite  $V_C C_{Si}$  in 3C-SiC; besides total spin  $S$  and symmetry, the charge transition level (CTL) into the respective charge state is given. Our calculated CTLs (see also Fig. 3) are about 0.2 eV lower as reported in Ref. [46]. Nonetheless, the negative charge states remain unstable ( $2^-$ ) or at least metastable ( $-$ ).

Charge state	+	0	-
Spin $S$	1/2	1	1/2
(Point group) symmetry	$C_{3v}$	$C_{1h}(C_{3v} - 85 \text{ meV})$	$C_{1h}(C_{3v} - 88 \text{ meV})$
Charge transition levels	$(2+ / +) = 1.57 \text{ eV}$	$(+ / 0) = 2.24 \text{ eV}$	$(0 / -) = 2.39 \text{ eV}$

TABLE IV. Spin-Hamiltonian (EPR) parameters of the  $V_C C_{Si}$  ( $S = 1/2$ ) centers in 3C-SiC: experimental data (see Fig. 3) compared with calculated values,  $g$  tensors, and  $^{29}\text{Si}$ -related hf splittings. For  $V_C C_{Si}^-$  the latter originate from the three (in  $C_{3h}$  symmetry) nonequivalent Si dangling bond atoms; in the case of  $V_C C_{Si}^+$  they perfectly fit to the experimental data and belong to the three Si atoms back-bonded to the three carbon ligands of the  $C_{Si}$  (see Fig. 2, right).

$V_C C_{Si}$	Total spin $S$ , symmetry	$g$ tensor	hf ( $^{29}\text{Si}$ ) ( $10^{-4} \text{ cm}^{-1}$ )
Experiment	$S = 1/2$	$g_{\parallel 111} = 2.0023$	$A_{\parallel 111} = 22.3$
	$C_{3v}$	$g_{\perp 111} = 2.0037$	$A_{\perp 111} = 18.1$
Theory $V_C C_{Si}^+$	$S = 1/2$	$g_{\parallel 111} = 2.0025$	$3 \times \text{Si}$
	$C_{3v}$	$g_{\perp 111} = 2.0041$	$A_{33} = 22.7$
			$A_{22} = 19.1$
			$A_{11} = 18.7$
Theory $V_C C_{Si}^-$	$S = 1/2$	$g_{11} = 2.0024$	$1 \times \text{Si}$
	$C_{3h}$	$g_{22} = 2.0028$	$A_{33} = 14.9$
		$g_{33} = 2.0068$	$A_{22} = 12.1$
			$A_{11} = 17.8$
			$2 \times \text{Si}$
			$A_{11} = -76.4$
			$A_{22} = -75.5$
			$A_{33} = -100.6$

intracenter photoluminescence (PL) transition highly improbable. Finally, the observation of the “ $E$ ” line PL in as-irradiated, nonannealed bulk samples [48] is also not coherent with our results that the  $V_C C_{Si}$  center is only generated by high-temperature annealing. Thus the origin of the single-photon emitter should be reconsidered.

## V. CONCLUSIONS

We have identified by EPR spectroscopy the carbon monovacancy defect in the  $1+$  charge state in 3C-SiC. Similar to the case of the isostructural defect  $V_{Si}^+$  (G1) in silicon, the positively charged carbon vacancy,  $V_C^+$ , is a negative- $U$  center resulting from strong pairwise coupling of the Si dangling bonds. Our modeling shows that the neutral carbon vacancy in 3C-SiC displays an exceptionally strong Jahn-Teller effect, much larger than in the 4H-SiC polytype and even larger than the isostructural vacancy in silicon. The carbon vacancy-carbon antisite defect is not a primary radiation-induced center but results from the structural instability of the silicon vacancy at temperatures above  $\geq 700^\circ\text{C}$ . The donor character of the  $V_C$  center will not allow its use for the growth of undoped semi-insulating samples contrary to the hexagonal polytypes, in which due to the higher band gaps a deep acceptor state is stabilized.

- [1] H. Itoh, A. Kawasuso, T. Oshima, M. Yoshikawa, I. Nashiyama, S. Tanigawa, S. Misawa, H. Okumura, and S. Yoshida, Intrinsic defects in cubic silicon carbide, *Phys. Status Solidi A* **162**, 173 (1997).
- [2] E. Sörman, N. T. Son, W. M. Chen, O. Kordina, C. Hallin, and E. Janzen, Silicon vacancy related defect in 4H and 6H SiC, *Phys. Rev. B* **61**, 2613 (2000).
- [3] N. Mizuochi, S. Yamasaki, H. Takizawa, N. Morishita, T. Oshima, H. Itoh, and J. Isoya, Continuous and pulsed EPR study of the negatively charged silicon vacancy with  $S = 3/2$  and  $C_{3v}$  symmetry in  $n$ -type 4H-SiC, *Phys. Rev. B* **66**, 235202 (2002).
- [4] T. T. Petrenko, T. L. Petrenko, and V. Ya Bratus, The carbon (100) split interstitial in SiC, *J. Phys.: Condens. Matter* **14**, 12433 (2002).
- [5] V. Y. Bratus, T. T. Petrenko, S. M. Okulov, and T. L. Petrenko, Positively charged carbon vacancy in three inequivalent lattice sites of 6H-SiC: Combined EPR and density functional theory study, *Phys. Rev. B* **71**, 125202 (2005).
- [6] J. Isoya, T. Umeda, N. Mizuochi, N. T. Son, E. Janzen, and T. Ohshima, EPR identification of intrinsic defects in SiC, *Phys. Status Solidi B* **245**, 1298 (2008).
- [7] N. T. Son, X. T. Trinh, L. S. Lovlie, B. G. Svensson, K. Kawahara, J. Suda, T. Kimoto, T. Umeda, J. Isoya, T. Makino, T. Ohshima, and E. Janzen, Negative- $U$  System of Carbon Vacancy in 4H-SiC, *Phys. Rev. Lett.* **109**, 187603 (2012).
- [8] V. Ya Bratus, R. S. Melnyk, B. D. Shanina, and S. M. Okulov, Thermal annealing and evolution of defects in neutron irradiated cubic SiC, *Semicond. Phys., Quantum Electron. Optoelectron.* **18**, 403 (2015).
- [9] H. J. Bardeleben, *Magnetic Resonance in Semiconductors and Nanostructures*, Springer Series in Materials Science Vol. 253, edited by P. Baranov, H. J. von Bardeleben, J. Jeleszko, and J. Wrachtrup (Springer-Verlag, Austria, 2017), Chap. 3.
- [10] A. Zywiets, J. Furthmüller, and F. Bechstedt, Vacancies in SiC: Influence of Jahn-Teller distortions, spin effects, and crystal structure, *Phys. Rev. B* **59**, 15166 (1999).
- [11] T. T. Petrenko, T. L. Petrenko, V. Ya, Bratus, and J. L. Monge, Symmetry, spin state and hyperfine parameters of vacancies in cubic SiC, *Appl. Surf. Sci.* **184**, 273 (2001).
- [12] L. Torpo, T. E. M. Staab, and R. M. Nieminen, Divacancy in 3C and 4H-SiC: An extremely stable defect, *Phys. Rev. B* **65**, 085202 (2002).
- [13] M. Bockstedte, M. Heid, and O. Pankratov, Signature of intrinsic defects in SiC: Ab initio calculations of hyperfine tensors, *Phys. Rev. B* **67**, 193102 (2003).
- [14] F. Bruneval, Methodological aspects of the GW calculation of the carbon vacancy in 3C-SiC, *Nucl. Instrum. Methods Phys. Res., Sect. B* **277**, 77 (2012).
- [15] J. Coutinho, V. J. B. Torres, K. Demmouche, and S. Öberg, Theory of the carbon vacancy defect in 4H-SiC: Crystal field and pseudo Jahn-Teller effects, *Phys. Rev. B* **96**, 174105 (2017).
- [16] D. D. Awschalom, R. Hanson, J. Wrachtrup, and B. B. Zhou, Quantum technologies with optically interfaced solid-state spins, *Nat. Photonics* **12**, 516 (2018).
- [17] M. Atatüre, D. Englund, N. Vamivakas, S. Y. Lee, and J. Wrachtrup, Material platforms for spin based photonic quantum technologies, *Nat. Rev. Mater.* **3**, 38 (2018).
- [18] S. E. Economou and P. Dev, Spin Photon entanglement interfaces in silicon carbide defect centers, *Nanotechnology* **27**, 504001 (2016).

- [19] D. J. Christl, P. V. Klimov, C. F. de las Casas, K. Szász, V. Ivády, V. Jokubavicius, J. Ul Hassan, M. Syväjärvi, W. F. Koehl, T. Ohshima, N. T. Son, E. Jánzén, A. Gali, and D. D. Awschalom, Isolated spin qubits in SiC with a high-fidelity infrared spin-to-photon interface, *Nat. Mater.* **14**, 160 (2015).
- [20] H. Seo, A. L. Falk, P. V. Klimov, K. C. Miao, G. Galli, and D. D. Awschalom, Quantum decoherence dynamics of divacancy spins in silicon carbide, *Nat. Commun.* **7**, 12935 (2016).
- [21] H. J. von Bardeleben, J. L. Cantin, A. Csóré, A. Gali, E. Rauls, and U. Gerstmann, NV centers in 3C, 4H, and 6H silicon carbide: A novel platform for solid-state qubits and nanosensors, *Phys. Rev. B* **94**, 121202(R) (2016).
- [22] S. A. Zargaleh, S. Hameau, B. Eble, F. Margailan, H. J. von Bardeleben, and W. Gao, Nitrogen vacancy center in cubic silicon carbide: A promising qubit in the 1.5  $\mu\text{m}$  spectral range for photonic quantum networks, *Phys. Rev. B* **98**, 165203 (2018).
- [23] J. F. Wang *et al.*, Coherent control of nitrogen-vacancy center spins in silicon carbide at room temperature, [arXiv:1909.12481](https://arxiv.org/abs/1909.12481) [Phys. Rev. Lett. (to be published)].
- [24] H. Kraus, V. A. Soltanov, F. Fuchs, D. Simin, A. Sperlich, P. G. Baranov, G. V. Astakhov, and V. Dyakonov, Magnetic field and temperature sensing with atomic-scale spin defects in silicon carbide, *Sci. Rep.* **4**, 5303 (2014).
- [25] Yu Zhou, J. Wang, X. Zhang, Ke Li, J. Cai, and W. Gao, Self-Protected Thermoemetry with Infrared Photons and Defect Spins in SiC, *Phys. Rev. Appl.* **8**, 044015 (2017).
- [26] S. Castelletto, B. C. Johnson, C. Zachreson, D. Beke, I. Balogh, T. Ohshima, I. Aharonovich, and A. Gali, Room temperature quantum emission from cubic silicon carbide nanoparticles, *ACS Nano* **8**, 7938 (2014).
- [27] V. Grachev, [www.visual-epr.com](http://www.visual-epr.com).
- [28] P. Giannozzi *et al.*, Quantum ESPRESSO: A modular and open-source software project for quantum simulations of materials, *J. Phys.: Condens. Matter* **21**, 395502 (2009).
- [29] P. Giannozzi *et al.*, Advanced capabilities for materials modeling with Quantum ESPRESSO, *J. Phys.: Condens. Matter* **29**, 465901 (2017).
- [30] J. P. Perdew, K. Burke, and M. Ernzerhof, Generalized Gradient Approximation Made Simple, *Phys. Rev. Lett.* **77**, 3865 (1996).
- [31] J. C. Slater, Statistical exchange-correlation in the self-consistent field, *Adv. Quantum Chem.* **6**, 1 (1972).
- [32] S. Sanna, Th. Frauenheim, and U. Gerstmann, Validity of the Slater-Janak transition-state model within the LDA+ $U$  approach, *Phys. Rev. B* **78**, 085201 (2008).
- [33] H. J. von Bardeleben, J. L. Cantin, U. Gerstmann, A. Scholle, S. Greulich-Weber, E. Rauls, M. Landmann, W. G. Schmidt, A. Gentils, J. Botsoa, and M. F. Barthe, Identification of the Nitrogen Split Interstitial(N-N)<sub>N</sub>in GaN, *Phys. Rev. Lett.* **109**, 206402 (2012).
- [34] J. Heyd, G. E. Scuseria, and M. Ernzerhof, Hybrid functional based on a screened Coulomb potential, *J. Chem. Phys.* **118**, 8207 (2003).
- [35] S. Greulich-Weber, EPR and ENDOR investigations of shallow impurities in SiC polytypes, *Phys. Status Solidi A* **162**, 95 (1997).
- [36] G. D. Watkins, Intrinsic defects in silicon, *J. Phys. Soc. Jpn.* **18**, 22 (1963).
- [37] M. Sprenger, S. H. Muller, E. G. Sieverts, and C. A. J. Ammerlaan, Vacancy in silicon: Hyperfine interactions from electron nuclear double resonance measurements, *Phys. Rev. B* **35**, 1566 (1987).
- [38] Y. Q. Jia and Guo-Gang Qin, Theoretical calculations of hyperfine interactions of the Jahn-Teller distorted single vacancy in silicon, *Phys. Rev. B* **37**, 2605 (1988).
- [39] U. Gerstmann, E. Rauls, H. Overhof, and Th. Frauenheim, Do we really need configuration interaction theory to understand the negative vacancy in silicon? *Phys. B (Amsterdam, Neth.)* **308-310**, 497 (2001).
- [40] E. Rauls, Th. Lingner, Z. Hajnal, S. Greulich-Weber, Th. Frauenheim, and J. M. Spaeth, Metastability of the neutral silicon vacancy in 4H-SiC, *Phys. Status Solid B* **217**, R1 (2000).
- [41] Th. Lingner, S. Greulich-Weber, J.-M. Spaeth, U. Gerstmann, E. Rauls, and H. Overhof, The annealing product of the silicon vacancy in 6H-SiC, *Phys. B (Amsterdam, Neth.)* **308-310**, 625 (2001).
- [42] M. Bockstedte, A. Mattausch, and O. Pankratov, *Ab initio* study of the annealing of vacancies and interstitials in cubic-SiC: Vacancy interstitial recombination and aggregation of carbon interstitials, *Phys. Rev. B* **69**, 235202 (2004).
- [43] U. Gerstmann, E. Rauls, and H. Overhof, Annealing of vacancy-related defects in semi-insulating SiC, *Phys. Rev. B* **70**, 201204(R) (2004).
- [44] E. Rauls, A. Gali, P. Deák, and Th. Frauenheim, The theoretical study of vacancy diffusion and vacancy-assisted clustering of antisites in SiC, *Phys. Rev. B* **68**, 155208 (2003).
- [45] R. Devanathan, W. J. Weber, and F. Gao, Atomic scale simulation of defect production in irradiated 3C-SiC, *J. Appl. Phys.* **90**, 2303 (2001).
- [46] F. Bruneval and G. Roma, Energetics and metastability of the silicon vacancy in cubic SiC, *Phys. Rev. B* **83**, 144116 (2011).
- [47] H. Itoh, N. Hayakawa, I. Nashiyama, and E. Sakuma, Electron spin resonance in electron irradiated 3C-SiC, *J. Appl. Phys.* **66**, 4529 (1989).
- [48] J. Lefevre, J. M. Constatini, S. Esnouf, and G. Petite, Silicon threshold displacement energy determined by photoluminescence in electron irradiated cubic SiC, *J. Appl. Phys.* **105**, 023520 (2009).